

*DRAFT COPY*

# Neutrino Fluxes, Hadron Production, and the Hadronic Hose

M. Messier

*Harvard*

J. Hlyen, A. Marchionni, S. Striganov

*Fermilab*

S. Kopp

*U. Texas, Austin*

G. Unel

*Northwestern*

## Abstract:

The hadronic hose is a proposed focusing system to be placed in the NuMI decay pipe. The hose, a single wire placed on the beam axis carrying a current of 1 kA, is expected to have two effects; 1) an increase in event rate in the MINOS detectors, and 2) an improvement in the near-to-far extrapolation of the neutrino spectrum. This note seeks to explain these two effects as well as provide a detailed comparison of the hose-on and hose-off fluxes for the three NuMI beams. Special attention is given to the low-energy beam.

## Contents

<b>1</b>	<b>Neutrino Fluxes</b>	<b>1</b>
1.1	Neutrino Fluxes With and Without Hadronic Hose . . . . .	1
1.1.1	Low Energy Beam . . . . .	1
1.1.2	Medium and High Energy Beam . . . . .	3
1.2	Sources of Flux Increase for PH2LE . . . . .	4
1.3	Effect of Design Parameters On Neutrino Flux . . . . .	11

<b>2</b>	<b>Hadron Production</b>	<b>14</b>
2.1	Hadron Production Data and NuMI/MINOS . . . . .	15
2.2	Simulations of Hadron Production on the NuMI Targets . . .	15
2.3	Uncertainties in the NuMI Neutrino Spectra . . . . .	21
2.3.1	Absolute Neutrino Flux Predictions . . . . .	21
2.3.2	Near – Far Relative Rates . . . . .	27
2.4	Conclusion . . . . .	31

	Low Energy Beam					
	$E < 6$ GeV			$E < 40$ GeV		
	LE	LE-HH	Increase	LE	LE-HH	Increase
GFLUKA	261.1	327.4	25.4%	473.5	731.9	54.6%
MARS	283.8	356.8	25.7%	443.7	655.3	47.7%
BMPT	241.6	303.7	25.7%	386.5	576.3	49.1%
MALENSEK	276.5	347.5	25.7%	488.8	720.6	47.4%

Table 1: Muon neutrino charged-current interaction rates at the far detector for the Low Energy beam with and without the hadronic hose. Results based on different simulations of the hadron production at the target are compared.

## 1 Neutrino Fluxes

### 1.1 Neutrino Fluxes With and Without Hadronic Hose

The affect of the hadronic hose [1, 2] on the neutrino fluxes has been calculated using a GEANT-based simulation of NuMI beamline. The simulation includes the central wire material, the lead and return wires, the central turning brackets, and a representative fraction of the spider supports. The magnetic field inside the decay pipe includes the fringe effects of the central, lead, and return wires. Simulations have been made for the low-energy, medium-energy, and high-energy beams neutrino beams. In this sections the fluxes for the low, medium, and high energy beam options are compared with and without the addition of the hadronic hose option.

#### 1.1.1 Low Energy Beam

Figure 1 shows the  $\nu_\mu$  charged-current event rates for the near and far detectors for the low energy beam with and with out the hose. At the far detector, the flux increase ranges from 20% to 50% below 6 GeV resulting in an overall increase in event rate of 25% below 6 GeV. The increase in the event rate in the high energy tail is roughly 75%. The reasons for these increases are discussed in Section 1.2.

Figure 2 show the  $\nu_e$  rates and fractions for the low-energy beams. The additional focusing of muons increases the  $\nu_e$  component of the beam. Below 6 GeV in the PH2LE beam the increase is roughly from 0.8% to 1.5% of the

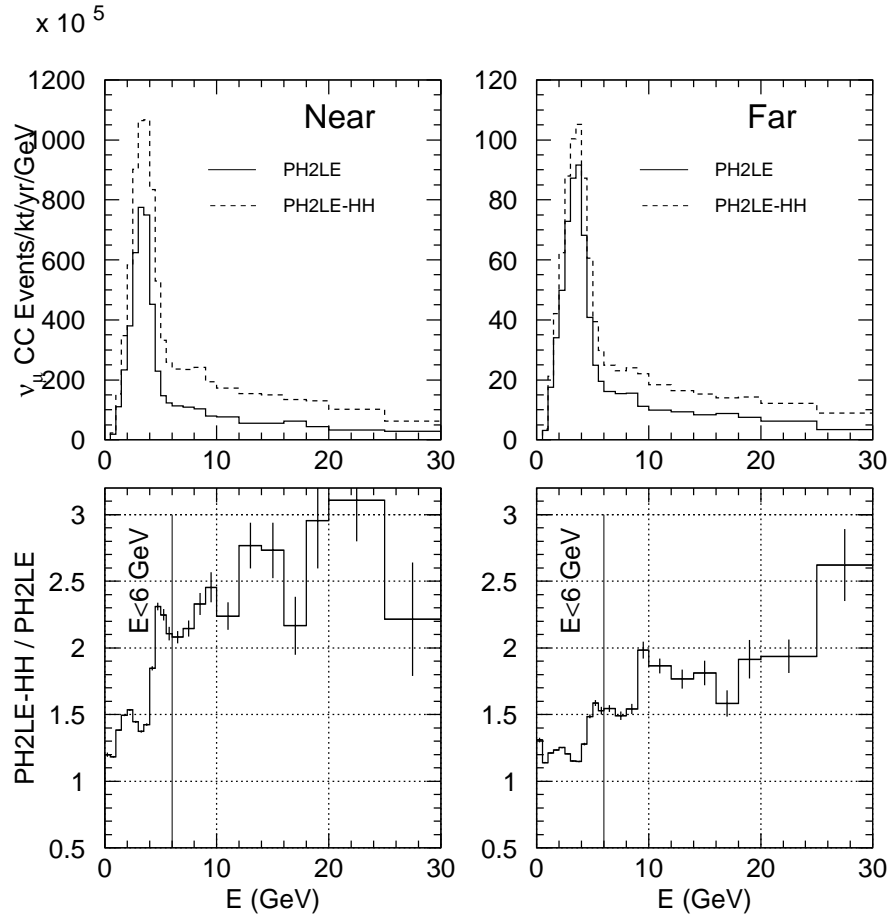


Figure 1: The  $\nu_\mu$  charged-current event rates at the far and near detectors. Bottom figures show the ratio of the hose-on flux (PH2LE-HH) to hose-off flux (PH2LE).

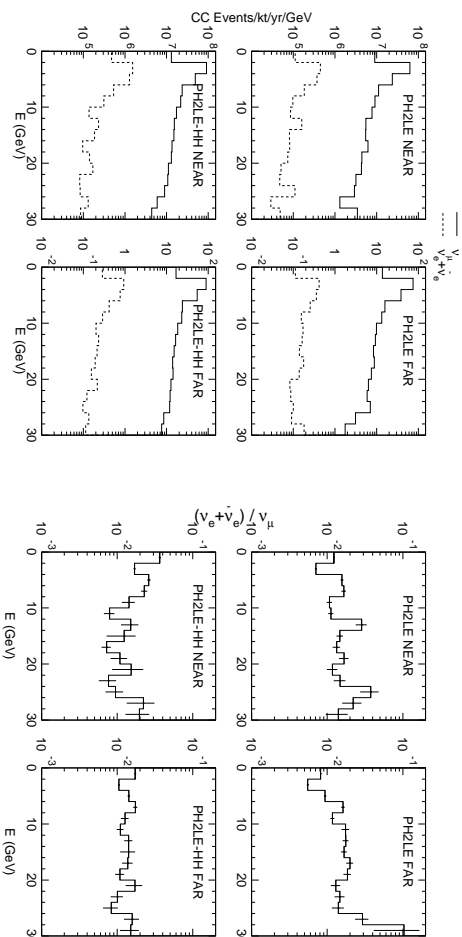


Figure 2: Left: The  $\nu_e$  rates at the near and far detectors for the PH2LE and PH2LE-HH beamlines. Right: The  $\nu_e$  fractions at the near and far detectors for the PH2LE and PH2LE-HH beamlines.

$\nu_\mu$  event rate at the far detector. Above 6 GeV the  $(\nu_e + \bar{\nu}_e)/\nu_\mu$  is roughly the same ( $\sim 1.5\%$ ) although slightly lower for the hose-on case than the hose-off case. The near detector sees a larger increase of the  $\nu_e$  component than the far detector. This is to be expected since the muons which are the source of the incense are focused and travel further down the decay pipe causing a significant increase in the solid angle subtended by the near detector. The increase is from roughly 1-2% hose-off to 2-3% hose on below 6 GeV. The fraction of  $\nu_e$  in the high energy tail is also larger, increasing from  $\sim 1\%$  to  $\sim 1.5\%$ .

### 1.1.2 Medium and High Energy Beam

Simulations of the hadronic hose have also been made for the medium and high-energy beam configurations. Tables 2 and 3 and Figures 3 5 summarize the muon neutrino event rates for the medium and high energy beams. The hose causes roughly a 20% increase in the medium energy neutrino rate and broadens the spectrum. Increases in the event rates for the high energy beam are only a few percent. However, the falling edge of the spectrum is significantly altered as the pion decay angles to the near and far detector

	Medium Energy Beam					
	$E < 14$ GeV			$E < 40$ GeV		
	ME	ME-HH	Increase	ME	ME-HH	Increase
GFLUKA	1077	1291	19.9%	1268	1675	32.1%
MARS	1178	1412	19.9%	1309	1647	25.8%
BMPT	996	1191	19.6%	1127	1419	25.9%
MALENSEK	984	1184	20.3%	1166	1510	29.5%

Table 2: Muon neutrino charged-current interaction rates at the far detector for the Medium Energy beam with and without the hadronic hose. Results based on different simulations of the hadron production at the target are compared.

are on average smaller resulting in neutrinos closer in energy to their pion parents.

The electron neutrino event rates are plotted in Figures 4 and 6. The electron neutrino fraction is roughly doubled in the medium energy beam below 10 GeV. Above 10 GeV the electron neutrino fraction is decreased by almost a factor two. The electron neutrino fractions in the high energy beam, follow a similar trend, as shown in Figure 6.

## 1.2 Sources of Flux Increase for PH2LE

The hadronic hose has the potential to increase the neutrino flux in the low energy beam by roughly 20-30% in the interesting energy range of 0-6 GeV. The flux increase can in part be understood by examining the distributions of the decay points of pions that produce neutrinos. Figure 7 shows the radial and  $p_t$  distributions of pions with momentum less than 14 GeV (which produce neutrinos in the range of 0-6 GeV) as they enter the decay pipe. Typical values for pions in this range are  $r < 30$  cm and  $p_t < 0.1$  GeV/ $c$ . At this distance the magnetic field created by the hadronic hose is strong enough to capture pions in orbits around the wire. Figure 9 shows several pion tracks calculated at  $r = 30$  cm,  $p = 14$  GeV/ $c$ , and  $p_t = 0.0, 0.028,$  and  $0.056$  GeV/ $c$ . In each case the pion was directed along the radial direction away from the beam axis (ie. worst case). The hose field is able to capture these pions out to about  $p_t = 0.05$  GeV/ $c$ . Also, while the pions with  $p_t = 0.056$  GeV/ $c$  are not captured in orbits, their time of flight is increased by roughly 40%

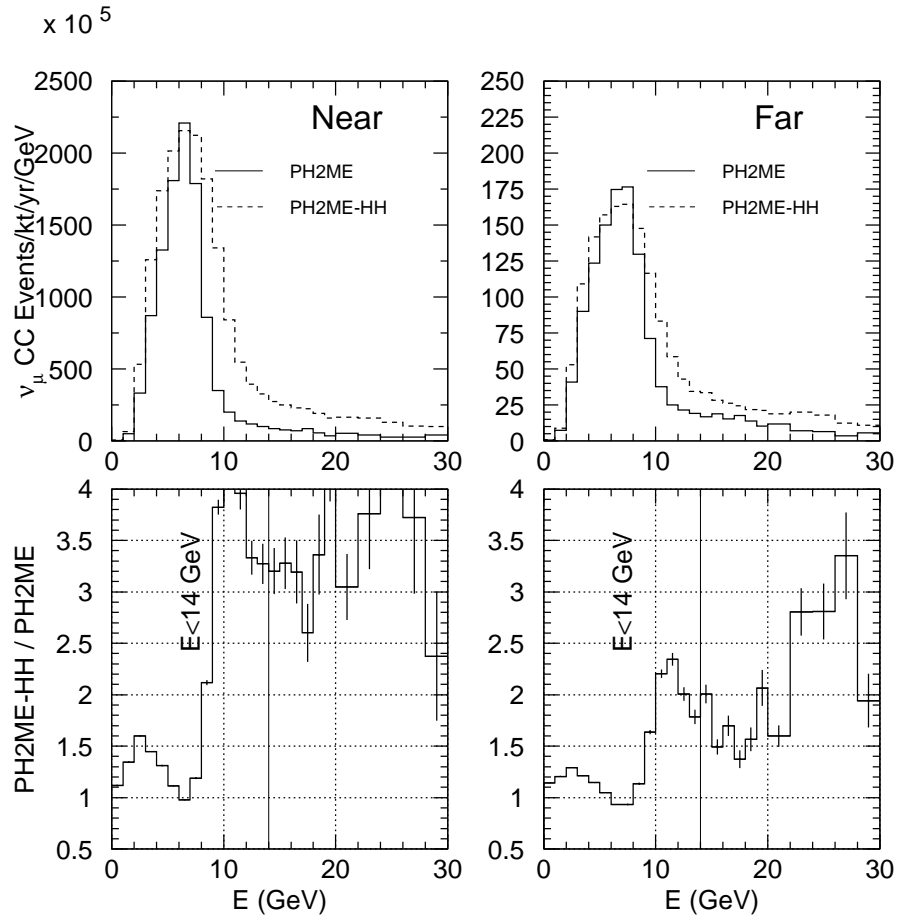


Figure 3: Comparison of the events rates with and with out the hose for the medium energy beam.

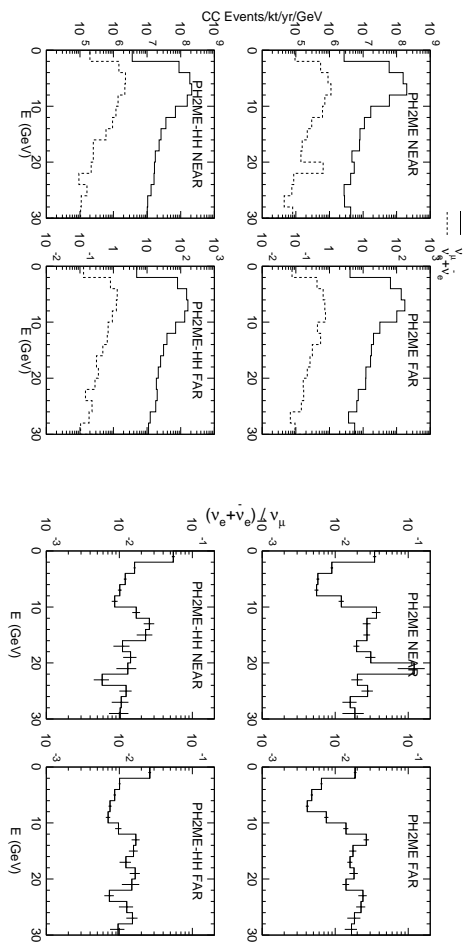


Figure 4: Electron neutrino event rates for the medium energy beam with and without the hadronic hose.

	High Energy Beam					
	$E < 30$ GeV			$E < 40$ GeV		
	ME	ME-HH	Increase	ME	ME-HH	Increase
GFLUKA	2694	2870	6.5%	2745	2983	8.7%
MARS	2513	2542	1.2%	2550	2598	1.9%
BMPPT	2432	2501	2.8%	2468	2555	3.5%
MALENSEK	2540	2593	2.1%	2578	2659	3.1%

Table 3: Muon neutrino charged-current interaction rates at the far detector for the Medium Energy beam with and without the hadronic hose. Results based on different simulations of the hadron production at the target are compared.

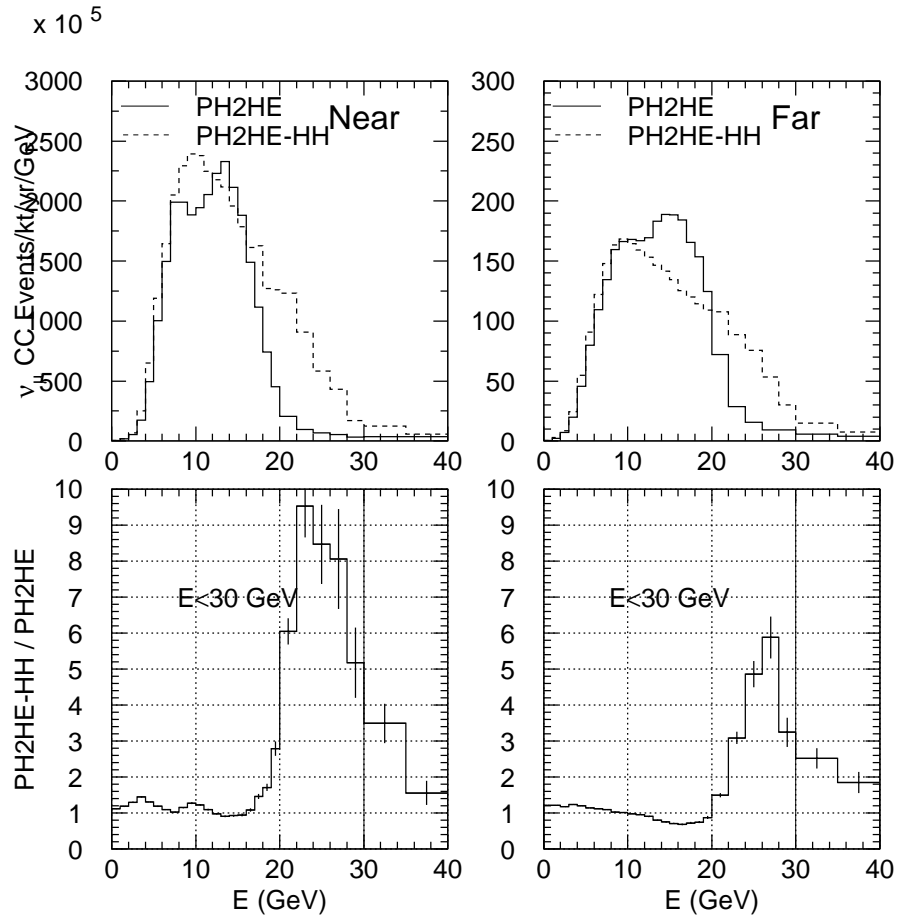


Figure 5: Comparison of the events rates with and with out the hose for the high energy beam.

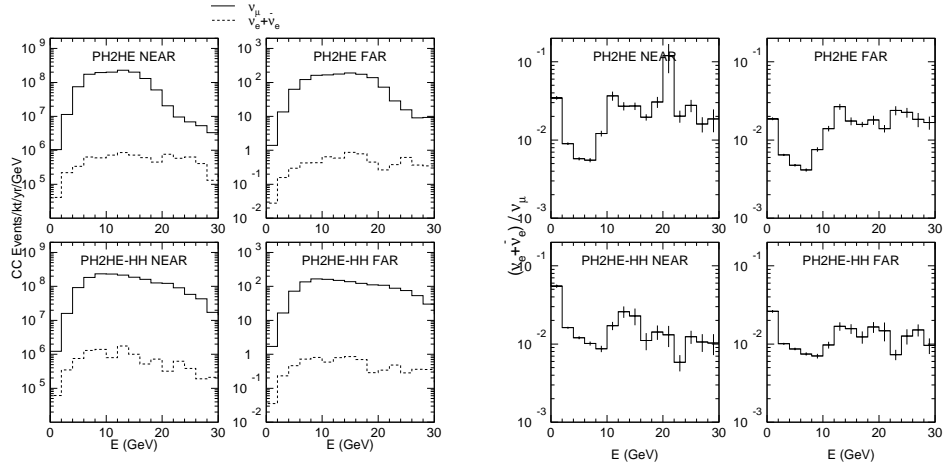


Figure 6: Electron neutrino rates for the high energy beam with and without the hadronic hose.

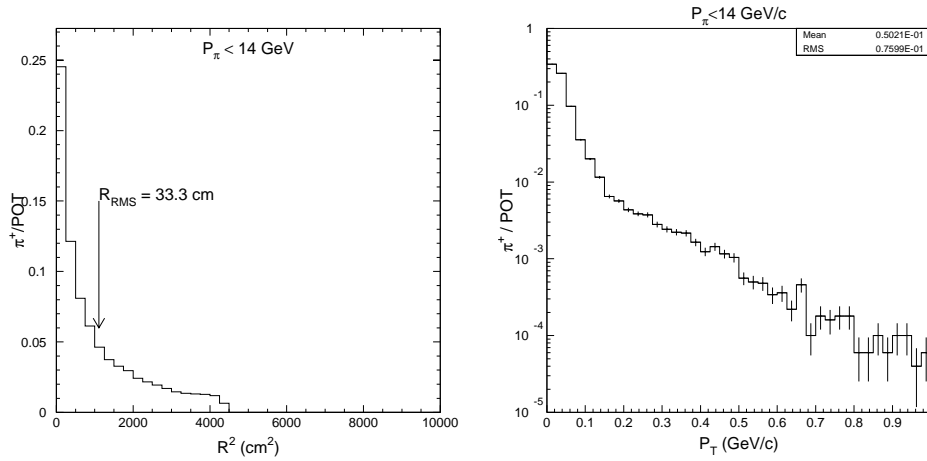


Figure 7: Left: Radial position of pions entering the decay pipe in the low energy beam configuration. Right: The transverse component of momentum of pions as they enter the decay pipe. Both figures are plotted only for pions with total momentum less than 14 GeV which are the pions which contribute to the neutrino flux between 0 and 6 GeV.

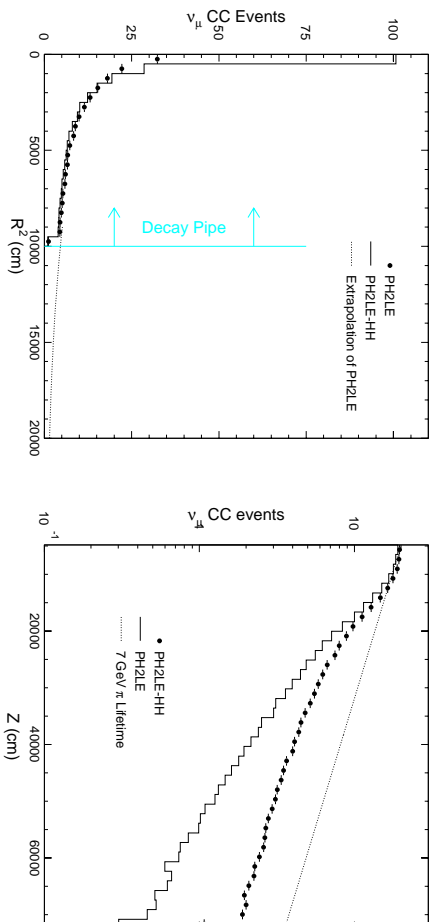


Figure 8: Left: The radial decay positions for pions that produce  $\nu_\mu$ . The decay pipe wall is at  $r^2 = 10000 \text{ cm}^2$ . Distributions for both the hose-on (PH2LE-HH) and hose-off (PH2LE) case are shown. Right: The  $z$  position of the decay positions for pions that produce  $\nu_\mu$ . For reference, a curve for a 7 GeV pion ( $\sim 3 \text{ GeV}$  neutrino) is also shown. The pion decays have been weighted by their contribution to the far detector event rate.

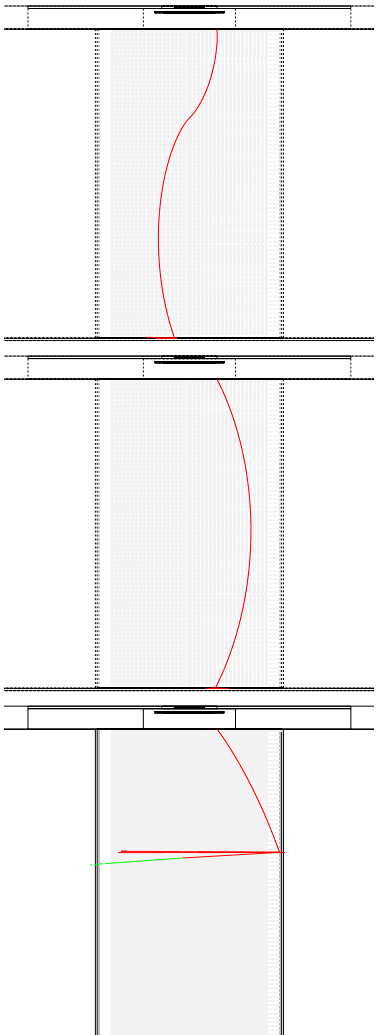


Figure 9: Pion tracks in the NuMI decay pipe for  $p = 14 \text{ GeV}/c$  and  $p_t = 0.0$  (left),  $0.028$  (center), and  $0.056$  (right)  $\text{GeV}/c$  entering the decay pipe at  $r = 30 \text{ cm}$ . The decay pipe is shown with compressed  $z$  scale; it is 1 m in radius and 675 m in length.

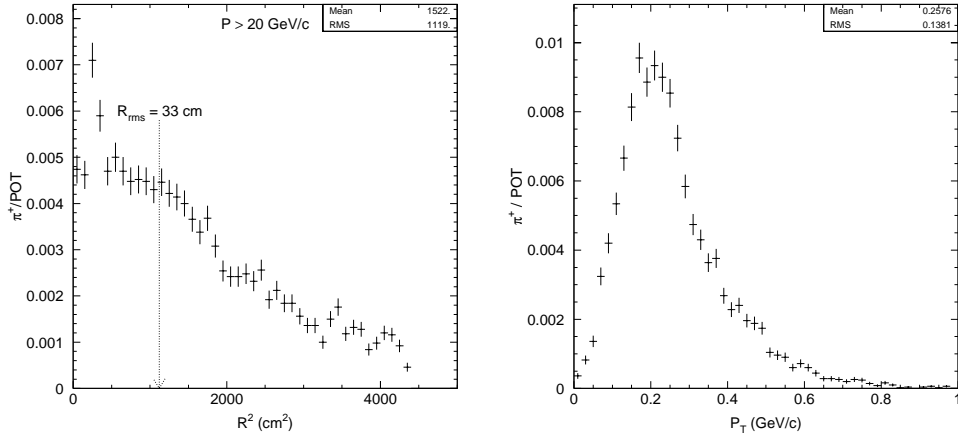


Figure 10: The radial and  $p_t$  distributions of pions entering the decay pipe. Pions which contribute to the high energy tail ( $p > 20$  GeV/c) have been selected.

from 550 ns with zero hose current to 760 ns with the hose current on. This additional focusing from the hose reduces the number of pions that interact on the decay pipe walls, increasing the flux. This can be seen by examining the distribution of decay vertices of pions which produce neutrinos. The decay vertex radial distributions for the hose-on and hose-off cases are shown in Figure 8. The increase at small radius can roughly be accounted for by the estimated area under the curve beyond the decay pipe wall. The focusing all results in more pion decays at large  $z$  as shown in Figure 8. With the hose off the number of pions decays decreases faster than one would expect based on the pion lifetime due to losses on the decay pipe walls. With the hose on the decay curve is close to parallel to the expectation based on the pion lifetime.

The flux increase in the high energy tail is expected to be larger than the increase in the peak region of the neutrino spectra. Figure 10 shows the distribution of pions which contribute to the high energy tail. As shown in Figure 11 the hose current bends 40 GeV these tracks back towards the axis out to a radius of about 30 cm. This bending has two affects on the neutrino flux. First, by bending tracks towards the beam axis pion losses on the decay pipe walls are reduced. Second, because the probability for a pion decay to

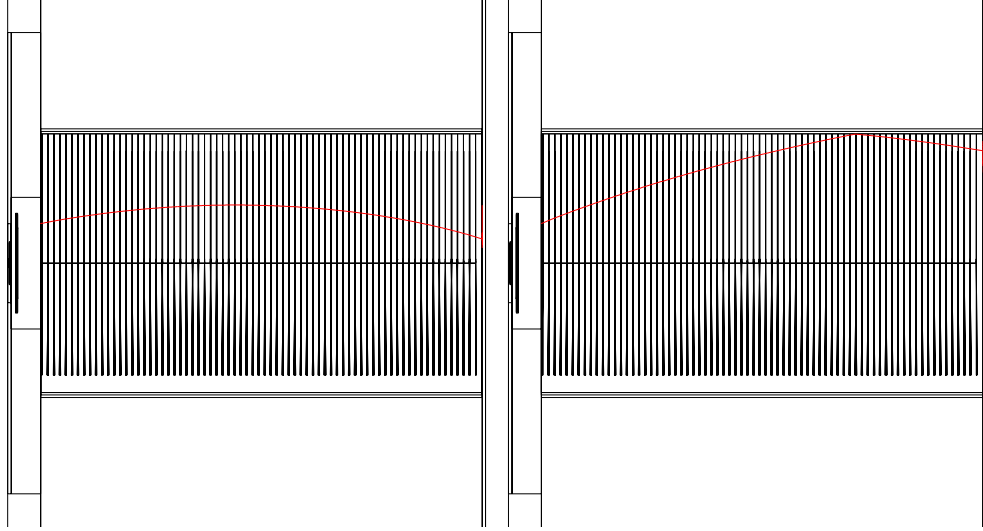


Figure 11: Pion trajectories entering the decay pipe at  $r = 30$  cm,  $p = 40$  GeV/ $c$  and  $p_t = 40$  MeV/ $c$ (left) and  $80$  MeV/ $c$  (right).

produce a neutrino traveling towards the far detector is proportional to

$$\frac{\gamma^2}{(1 + \gamma^2 \theta^2)^2}, \quad (1)$$

where  $\theta$  is the angle between the pion flight direction and the neutrino path to the detector, keeping pions close to the beam axis (small theta) increases the efficiency for pions to produce neutrinos traveling in the direction of the MINOS detectors.

### 1.3 Effect of Design Parameters On Neutrino Flux

There are several factors which affect the expected increase in flux for the low energy beam. The most straight forward of these is the hose current. The current design is to run the hose at 1 kA which is which results in a fairly comfortable wire temperature. This current could be increased at the expense of some safety. Figure 12 shows the increase in event rates in three energy ranges ( $E < 3$ ,  $3 < E < 6$ , and  $E > 6$  GeV) for the low energy beam. The increasing the wire current to 1.5 kA can increase the event rate an additional  $\sim 5\%$  below 6 GeV. Increases in the high energy tail are larger; roughly 30%.

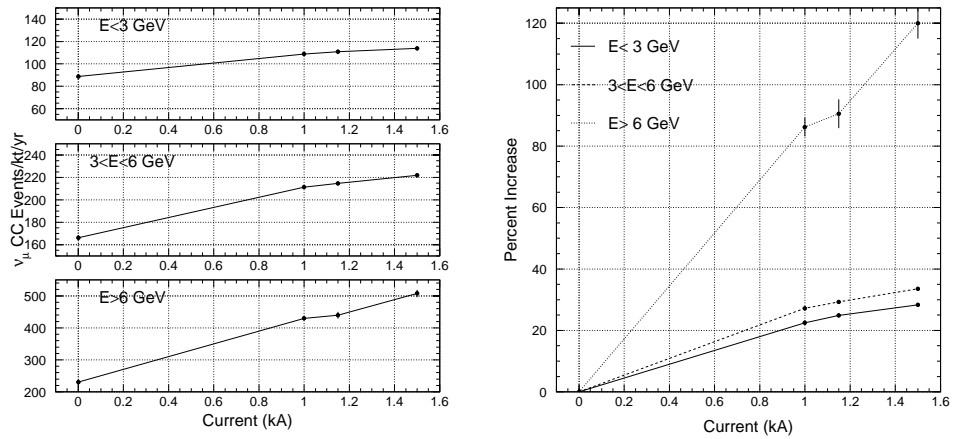


Figure 12: The low-energy beam event rates at the far detector as a function of wire current. Left: The number of events in the three bins as a function of wire current. Right: The percent increase in the bin content as a function of wire current.

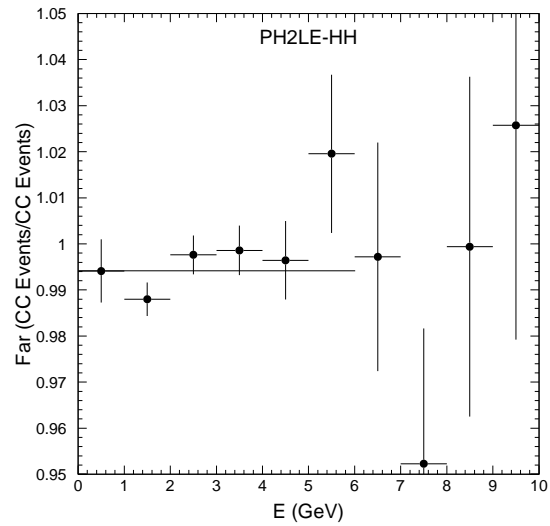


Figure 13: The decrease in neutrino flux due to the wire turning brackets as a function of energy for the low-energy beam.

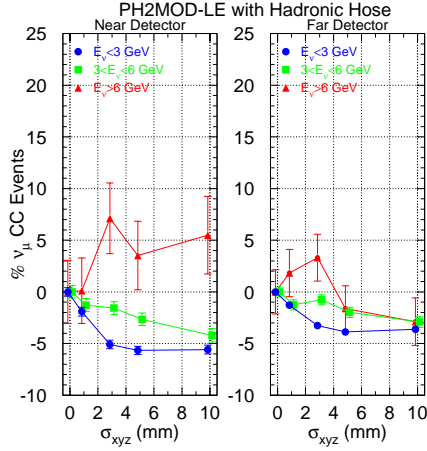


Figure 14: Affect of hadronic hose wire alignment on neutrino flux at the near and far detectors. Misalignments of a few mm result in roughly a 1-2% decrease in neutrino flux below 6 GeV.

The affect of the material in the neutrino beam has also been studied. Previously, the neutrino flux has been calculated neglecting the hose wire and turn-bracket material. This study indicated that the wire material results in roughly a 4% decrease in the neutrino flux in the peak energy region. This calculation was repeated including the wire material but neglecting the turning bracket material. Results are plotted in Figure 13. The turning brackets alone result in roughly a 0.6% decrease in the neutrino flux in the peak.

To date, the additional material in the decay pipe at large radius has been neglected. This material is less than 10 cm in radial extent and therefore its affect on neutrino flux must be orders of magnitude smaller than 5% which would result from decreasing the decay pipe radius by 10 cm [3].

Wire alignment also affects the expected neutrino flux. Figure 14 shows the change in the event rate at the far detector for various levels of wire misalignment. The current design keeps wire sag (a form of misalignment) to  $\sim 2$  mm. This is expected to result in a 2% decrease in the event rate below 6 GeV from the nominal 25% increase relative to the baseline PH2LE

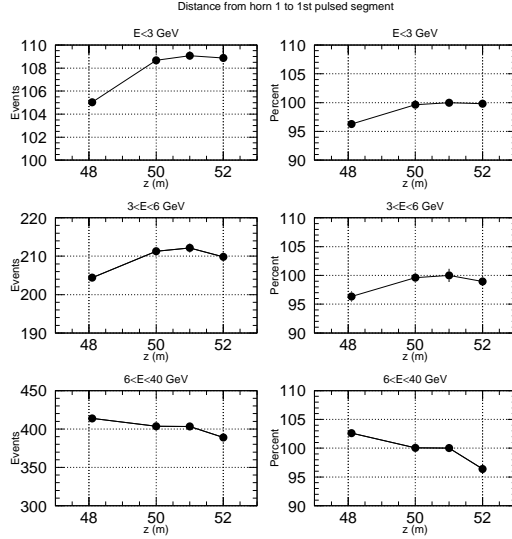


Figure 15: Change in the far detector flux as a function of the distance from the first horn to the start of the hadronic hose wire. Event rates are shown on the left for three energy bins ( $E < 3$  GeV,  $3 < E < 6$  GeV,  $6 < E < 40$  GeV). Changes in percent are shown at the right.

beamline.

The variation of neutrino flux with distance from the target to the first pulsed hose segment has also been examined. Figure 15 shows the change in neutrino interaction rates as the far detector as a function of the  $z$  position of the first pulsed hose segment. Placing the wire too close results in roughly a 4% loss. The current position of the hose wire ( $z = 50$  m) appears close to optimal although moving back another meter may have advantages.

## 2 Hadron Production

Secondary production of pions and Kaons is likely to be the largest uncertainty in the prediction of the NuMI neutrino spectra. This section reviews the available data and its relevance to the NuMI low, medium, and high-energy beams. The uncertainties in the absolute prediction and the relative Far-Near spectra due to uncertainties in hadron production are also estimated

Experiment	Interaction	$x_F$	$p_t$
Atherton et al. [4]	400 GeV/ $c$ p-Be	0.15 – 0.75	0 – 0.5 GeV/ $c$
Barton et al. [5]	100 GeV/ $c$ p-H,C,Al p-Cu,Ag,Pb	0.3 – 0.88	0.3 – 0.5 GeV/ $c$
SPY [6]	450 GeV/ $c$ p-Be	0.0 – 0.3	0.0 – 0.6 GeV/ $c$

Table 4: Summary of hadron production data.

for the three neutrino beams for the hose-on and hose-off cases.

## 2.1 Hadron Production Data and NuMI/MINOS

The prediction of secondary production on the NuMI target has large uncertainties due primarily to the lack of available data relevant to the NuMI case. The most relevant measurements are summarized in Table 4. Most of the available data was taken using Beryllium targets at significantly higher primary momentum and on shorter targets than will be used by NuMI. This requires extrapolation from Be to C, from 400 or 450 GeV/ $c$  to 120 GeV/ $c$  and from target lengths of roughly 0.5 m to 1.0 m. These extrapolations introduce roughly 15-20% uncertainties in the predictions of secondary production of protons on the NuMI targets.

Figures 16, 17, and 18 show the  $p$  and  $p_t$  distributions of pions at the target weighted by the number of neutrino interactions they produce at the near and far detectors. Superimposed on the  $p$  and  $p_t$  distributions are points measured by experiment. Note that while the target region for the low energy beam is bracketed by measurements from Ref.[6], measurements in the high energy tail ( $p > 20$  GeV/ $c$ ,  $p_t < 0.2$ ) are significantly more sparse. The region focused by the medium and high energy beams lies just outside the regions reported by Ref [6] and in a region where measurements from [5] and [4] are sparse.

## 2.2 Simulations of Hadron Production on the NuMI Targets

To estimate the impact of uncertainties in hadron production on NuMI-MINOS simulations of the NuMI targets have been made using the GEANT-FLUKA [7] (GFLUKA hereafter) and MARS [9] simulation codes. Addition-

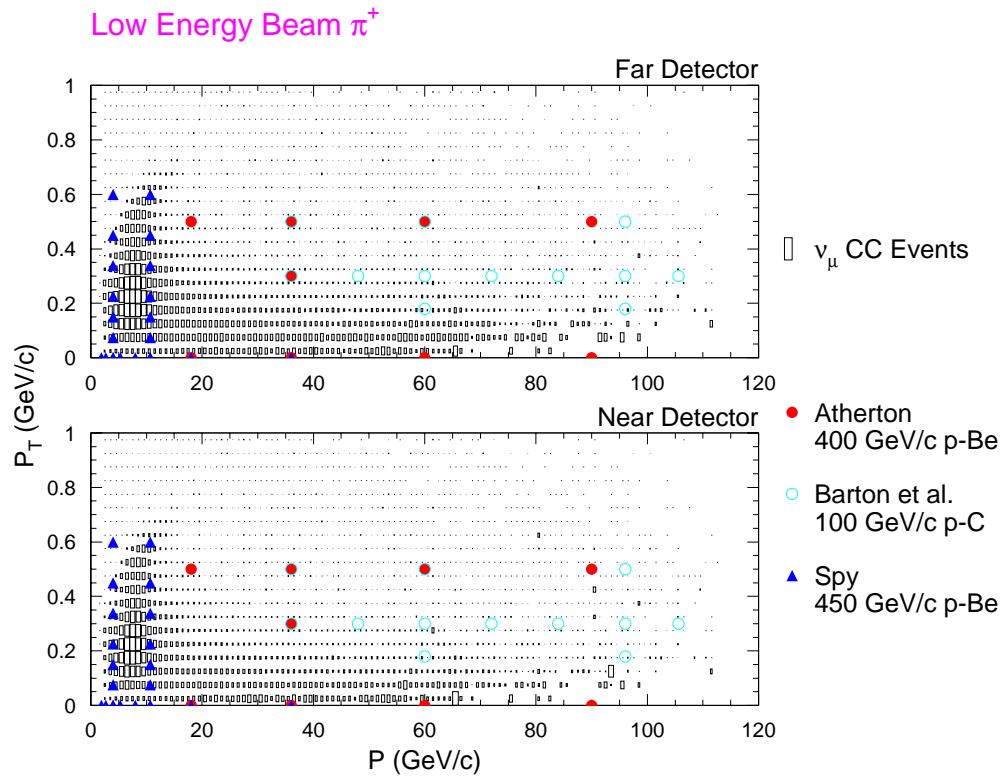


Figure 16: The  $p$  and  $p_t$  ranges of secondaries focused by the NuMI low-energy beam. Data from various hadron production experiments have been superimposed.

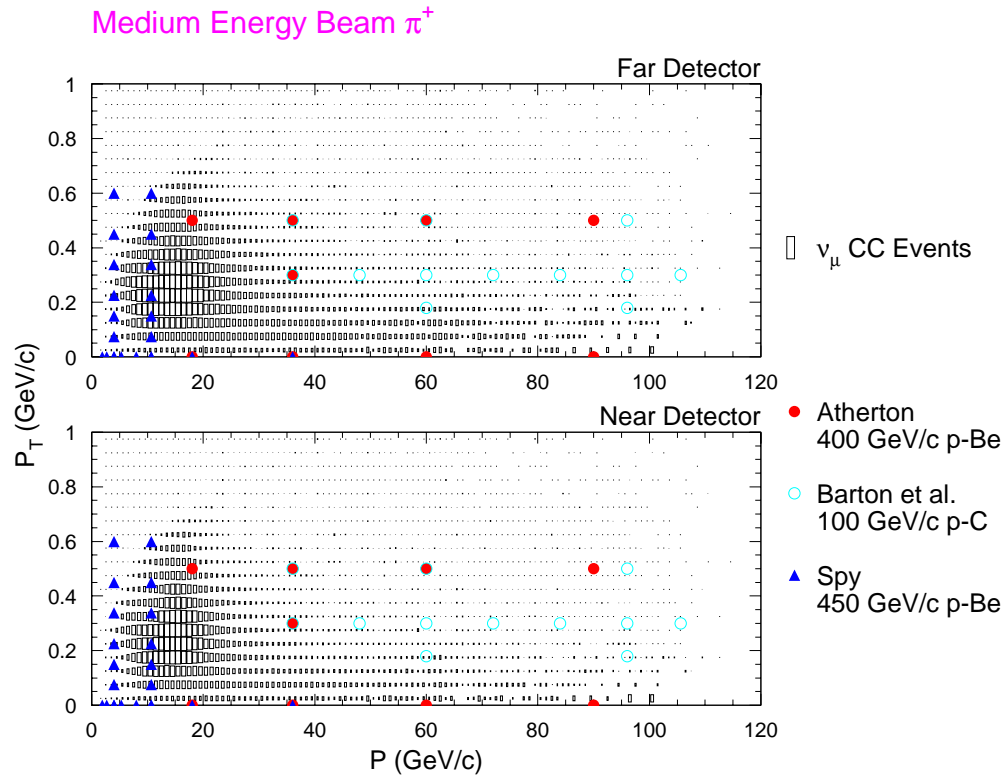
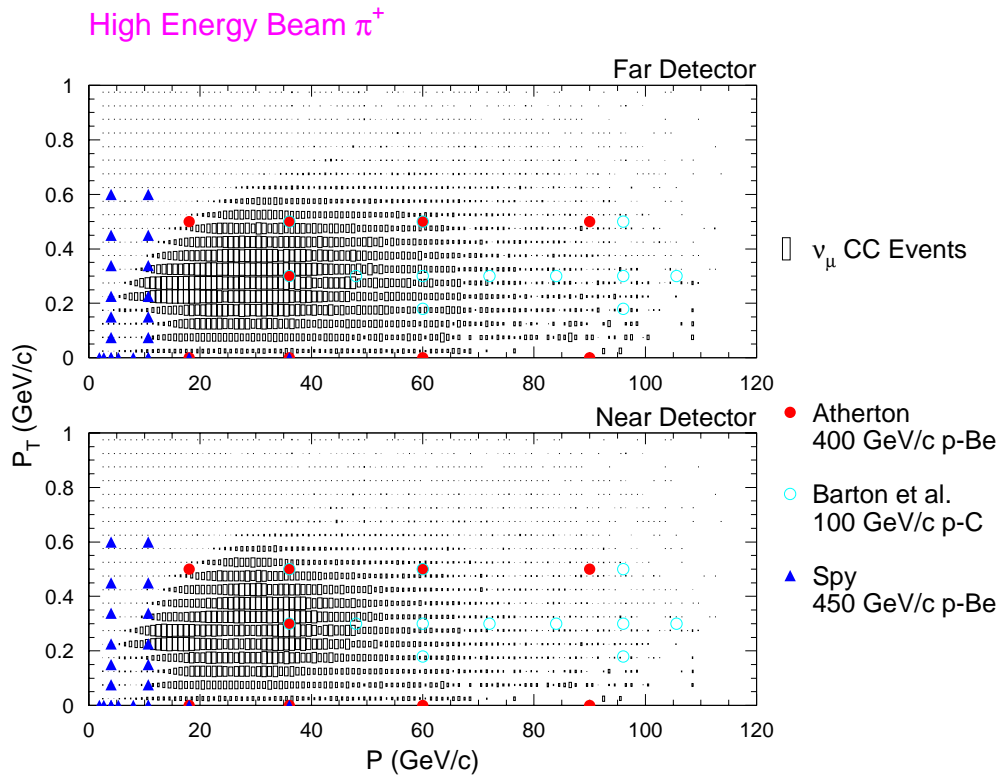


Figure 17: The  $p$  and  $p_t$  ranges of secondaries focused by the NuMI high-energy beam. Data from various hadron production experiments have been superimposed.



○

▲

Figure 18: The  $p$  and  $p_t$  ranges of secondaries focused by the NuMI medium-energy beam. Data from various hadron production experiments have been superimposed.

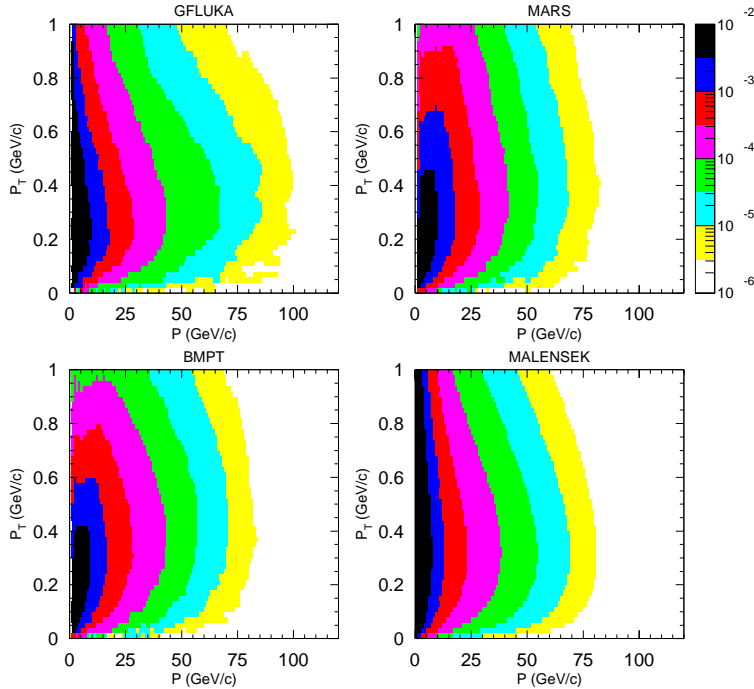


Figure 19: Number of pions produced on the NuMI low-energy target in units of  $\#/\text{POT}/\text{GeV}/0.2 \text{ GeV}/c$  as a function of pion momentum and transverse momentum. Yields for the GFLUKA, MARS, BMPT, and MALENSEK models are shown.

ally, the MARS code was modified to use the recent BMPT parameterization of the SPY and Atherton data [10]. Additionally, comparisons to the parameterization of the Atherton data for thick targets due to Malensek [8] have been made. Note that the Atherton data only reaches down to  $x_f$  of 0.15, and hence the Malensek parameterization should not be expected to extrapolate well to low  $x_f$  but should characterize the data reasonably at larger  $x_f$ . For compactness, I will refer to this collection of simulations and parameterizations as four “models” of hadron production, GFLUKA, MARS, BMPT, and MALENSEK.

Comparisons of the predicted yields from the NuMI target for these four models are shown in Figure 19. Differences in the models is typically 15-20%

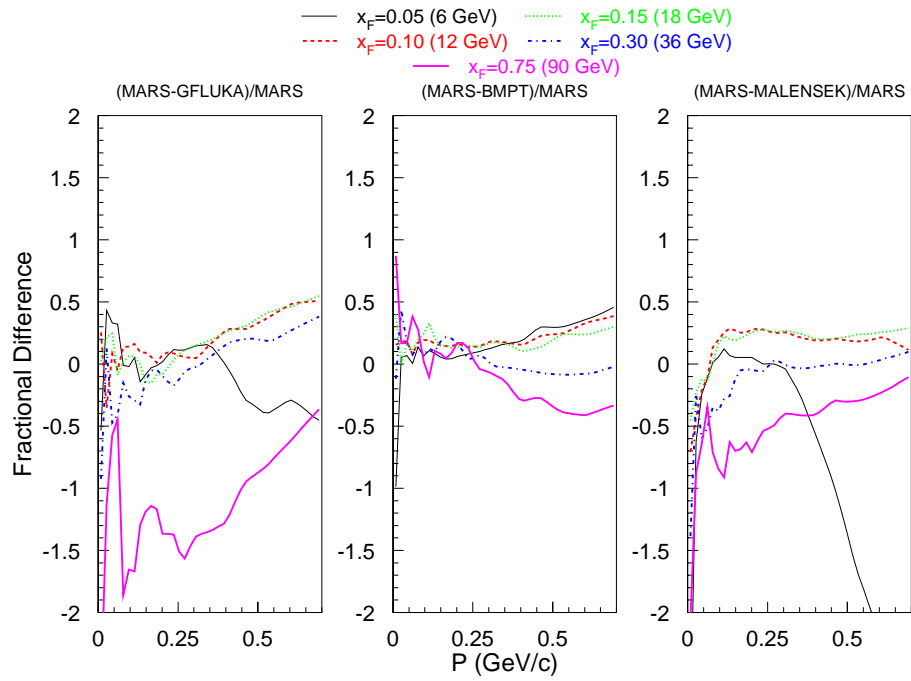


Figure 20: Comparison of the various simulations of the NuMI low-energy targets as a function of  $p_t$  for various values of  $x_F$ .

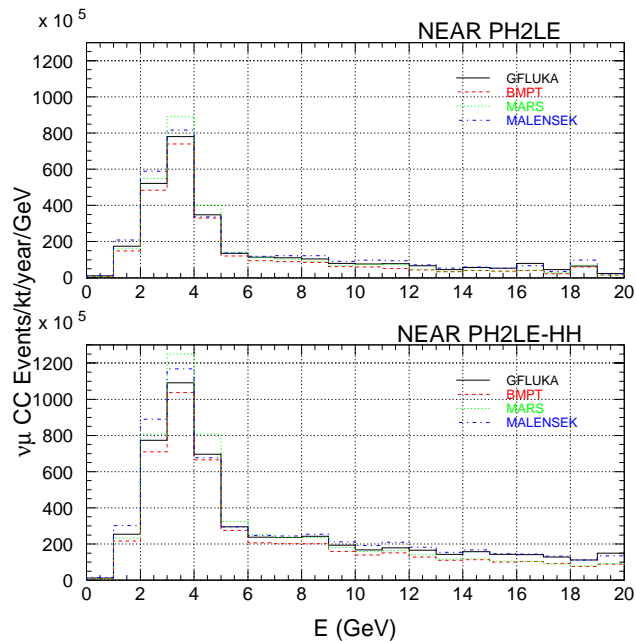


Figure 21: Near detector spectra for the low-energy beam hose-off (top) and hose-on (bottom) for various models of hadron production.

which larger errors in the extremes;  $p_t = 0$ ,  $p_t = 0.7$ , and large  $x_f$ .

## 2.3 Uncertainties in the NuMI Neutrino Spectra

### 2.3.1 Absolute Neutrino Flux Predictions

Figures 21, 22, and 23 compares the predictions of the absolute rates at the near detector for the low, medium and high energy beams using the GFLUKA, MARS, BMPT, and MALENSEK models of the NuMI targets. For the low energy beam, variations in the absolute rates are roughly 15% as shown in Figure 24. Variations for the medium and high-energy beams is shown in Figures 25 and 26; variations are also roughly 10-15%.

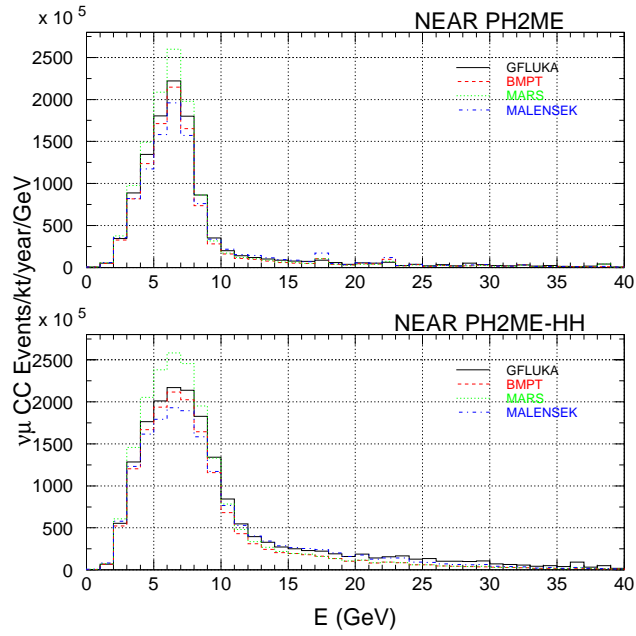


Figure 22: Near detector spectra for the medium-energy beam hose-off (top) and hose-on (bottom) for various models of hadron production.

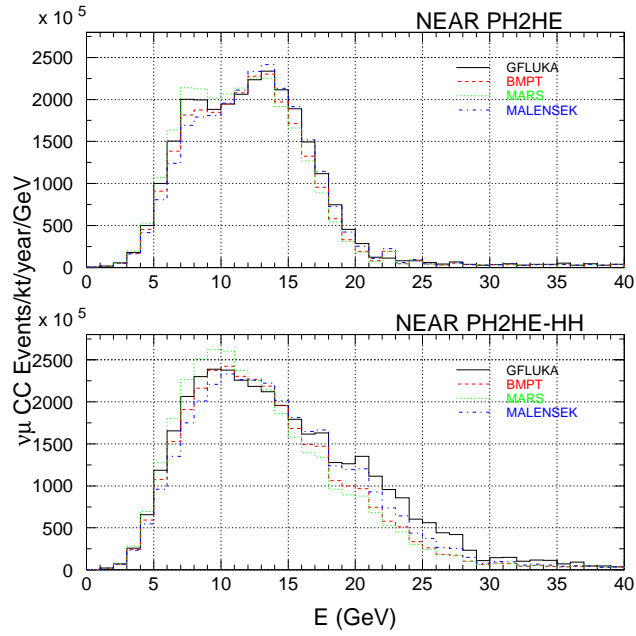


Figure 23: Near detector spectra for the high-energy beam hose-off (top) and hose-on (bottom) for various models of hadron production.

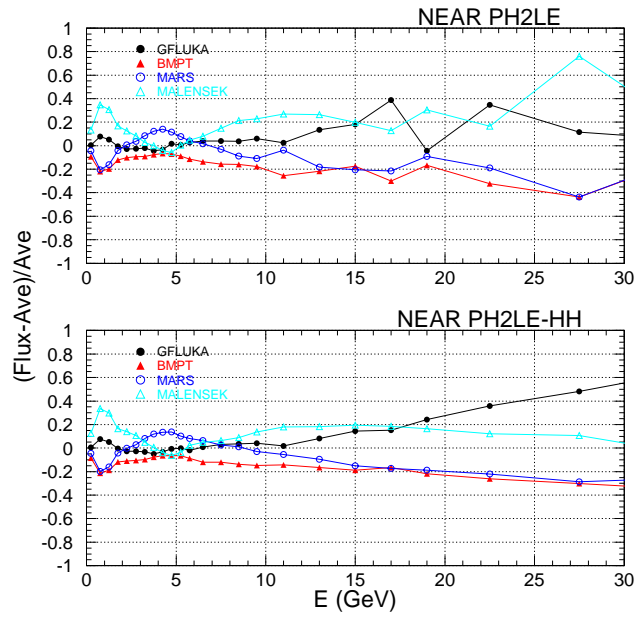


Figure 24: Comparisons of the predicted absolute near detector spectra for the low-energy beam using various hadron production models. The hose-off (top) and hose-on (bottom) cases are shown.

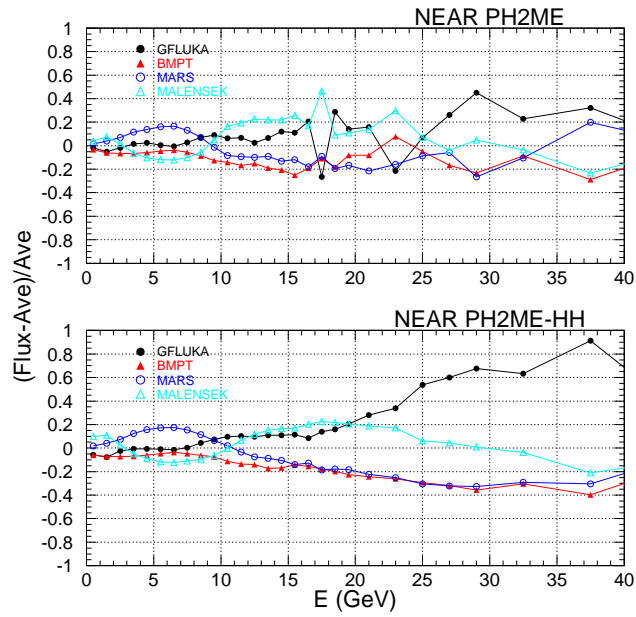


Figure 25: Comparisons of the predicted absolute near detector spectra for the medium-energy beam using various hadron production models. The hose-off (top) and hose-on (bottom) cases are shown.

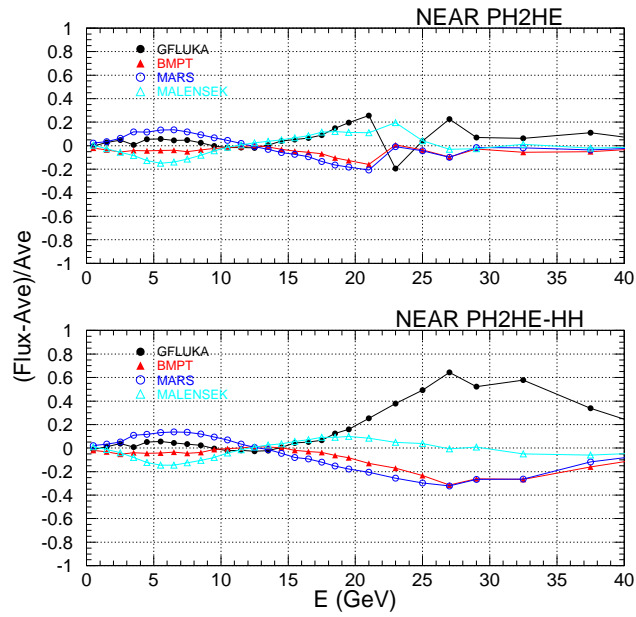


Figure 26: Comparisons of the predicted absolute near detector spectra for the high-energy beam using various hadron production models. The hose-off (top) and hose-on (bottom) cases are shown.

### 2.3.2 Near – Far Relative Rates

The MINOS experiment will compare the neutrino spectra at the far detector to the expected spectra based on the measurement of the spectra at the near detector. Any deviations due to neutrino oscillations will result in a difference between this predicted spectra and the observed.

The extrapolation of the near spectrum to the far spectrum is not simple. The distance to the far detector is roughly 1000 times larger than the length of the NuMI beamline (735 km vs. 0.725 km). Thus, to a very good approximation the far detector sees a point neutrino source. However, the near detector, which is located at 1.04 km, sees an extended source of neutrinos. In general, high energy pions decay closer to the near detector than low energy pions and hence one expects the Far/Near ratio to be larger at low energies than at high energies. Also, well focused pions travel further down the decay pipe than poorly focused pions which interact on the decay pipe wall before they decay. Thus one expects pions that have small  $p_t$ , or that are located near the beam axis, to contribute relatively more neutrinos to the near detector spectrum than pions with large  $p_t$  or large radius. Further, the decay angle to the near detector increases much more rapidly as the pion radius increases than does the angle to the far detector. These factors, pion  $p_t$ , and radial position, are dependent upon the initial conditions of the pions at the target, and hence upon the model of hadron production.

Figure 30 shows estimates of the Far/Near ratio using various hadron production models for the hose-on and hose-off cases. Without the hadronic hose, the far/near ratio exhibits several pronounced features. These features result from different trajectories of pions through the two horn system. Figure 27 illustrates five categories of pion trajectories. Pions can 1) travel through the neck of both horns, 2) travel through the neck of the first horn and be focused by the second horn, 3) be focused by the first horn and travel through the neck of the second horn, 4) be over focused by the first horn and focused by the second horn, and 5) be under focused by the first horn and focused by the second. Figure 28 shows the neutrino spectra resulting from these five classes of pion trajectories. The far/near ratios for the five cases are shown in Figure 29. All curves exhibit the general decay trend; any source of pions entering the decay pipe will produce more decays at the upstream end of the decay pipe (large distance to the near detector) than at the downstream end (small distance to the near detector). The peak of the neutrino spectrum is primarily due to over-focused pions. The feature in the

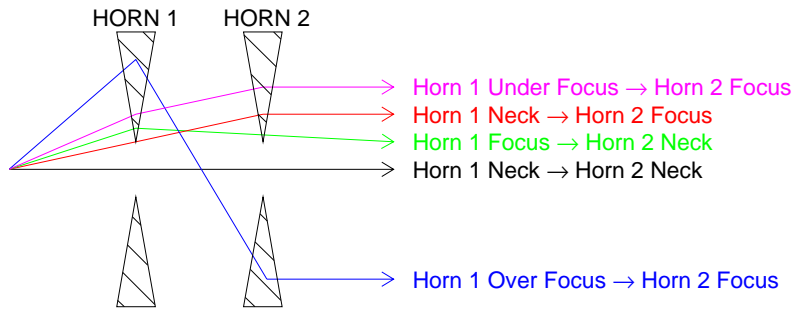


Figure 27: The different categories of the low-energy beam horn acceptances.

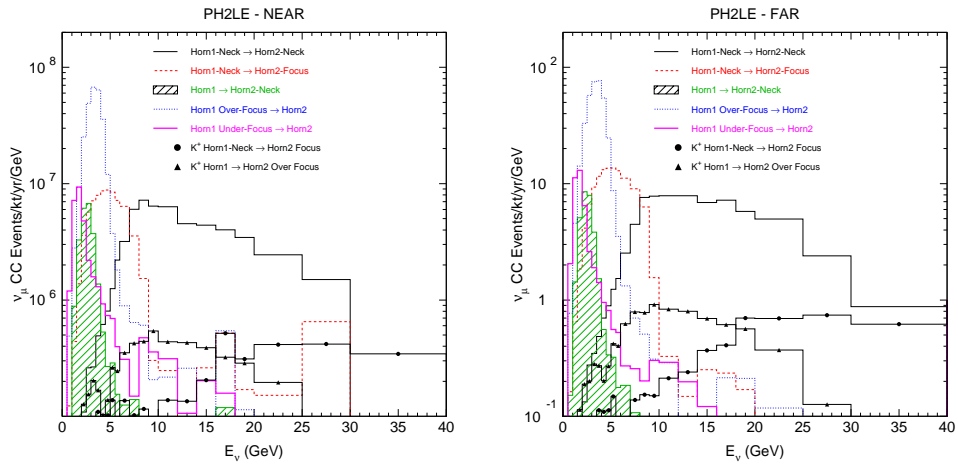


Figure 28: Muon neutrino spectra from pions and Kaons passing through different ranges of the low-energy beam horn acceptances.

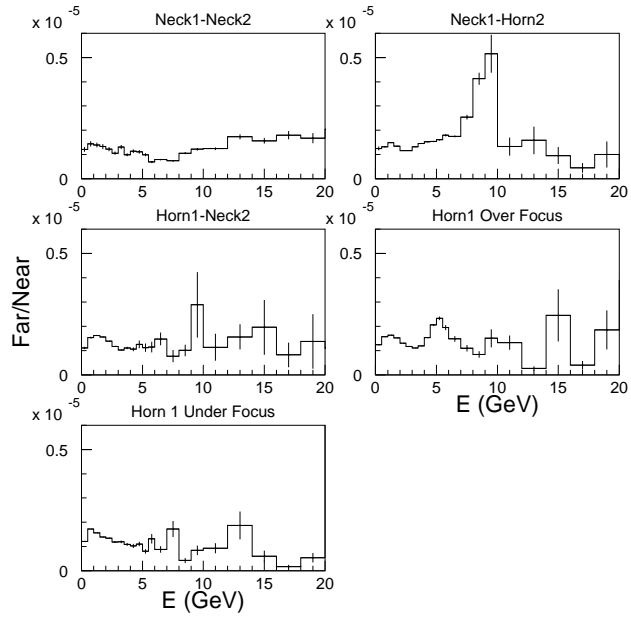


Figure 29: The far/near ratio for the five classes of pion trajectories contributing to the low-energy neutrino spectra.

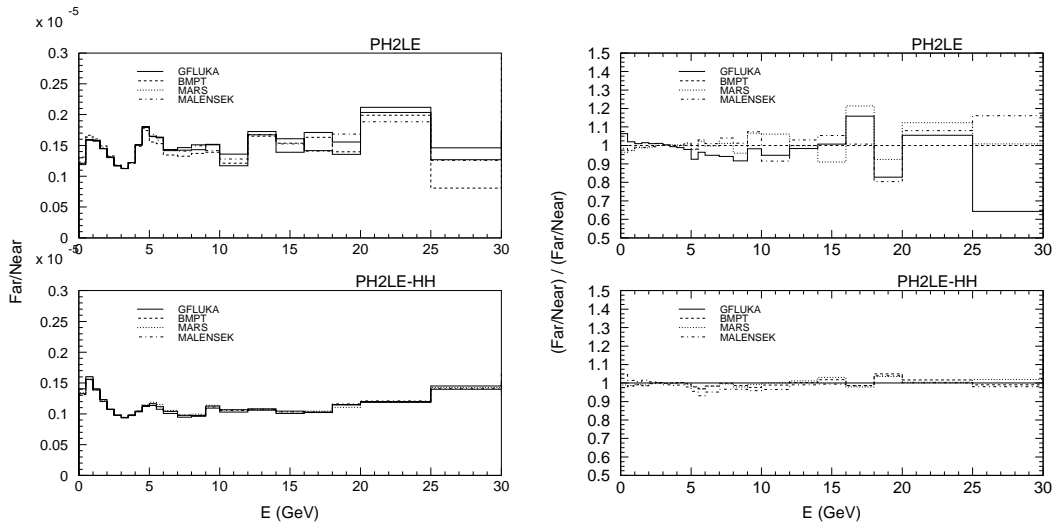


Figure 30: Left: The Far/Near ratio for the low-energy beam calculated using four models of hadron production on the NuMI target. Results for the hose-off (top) and hose-on (bottom) cases are shown. Right: Comparison of the Far/Near ratio for the various hadron production models relative to the Far/Near prediction from the GFLUKA model for the medium-energy beam. Results are shown for both the hose-off (top) and hose-on (bottom) cases.

far/near ratio at 4-5 GeV can be attributed to pions which are over-focused by the first horn. The rise in the far/near ratio approaching 10 GeV results from pions which only see focusing from horn two; these pions contribute the most neutrinos to the spectra in the range from 5-7 GeV. Starting around 8 GeV the neutrino spectrum is dominated by pions which travel through the necks of both horns. These pions see almost no horn focusing and are thus extremely sensitive to variations in the hadron production models, as seen in Figure 30.

The additional focusing of the hadronic hose allows more pions to decay before they interact bringing the far/near curves shown in Figure 30 closer to the simple prediction based on the pion lifetime and smoothes out the jumps in the hose-off case caused by the shifts between the different ranges of the horn acceptances. Also, as the hose keeps pion decays on average closer to the beam axis, and varies the decay angles to the near and far detectors, systematic differences in the near and far detector fluxes are largely averaged out. This modulation of the decay angles to the near and far detectors also reduces the model dependence of the far/near prediction as features in the far/near ratio introduced from variations of the production model integrate out.

## 2.4 Conclusion

The hadronic hose has the potential to increase the neutrino flux in both the low-energy beam (25%) and medium-energy beams (20%). These increases are not strongly dependent upon the particular hadron production model chosen, and include losses due to the hose wire material. Mis-alignments of the central hose wire of 2 mm (due to sag, for example) are estimated to result in roughly a 2% decrease in event rates. Additional hose hardware has been estimated to have only a very small effect on flux, less than 1%.

Uncertainties in the far/near ratio due to uncertainties in production of secondaries on the NuMI target range from roughly 1 – 4% in the peak of the low-energy beam to 5 – 10% in the high energy tail. The addition of the hadronic hose to the NuMI decay pipe reduces these uncertainties by roughly a factor of 2 to 3, in the low energy beam. Similar reductions in the far/near prediction are obtained for the medium and high-energy beams.

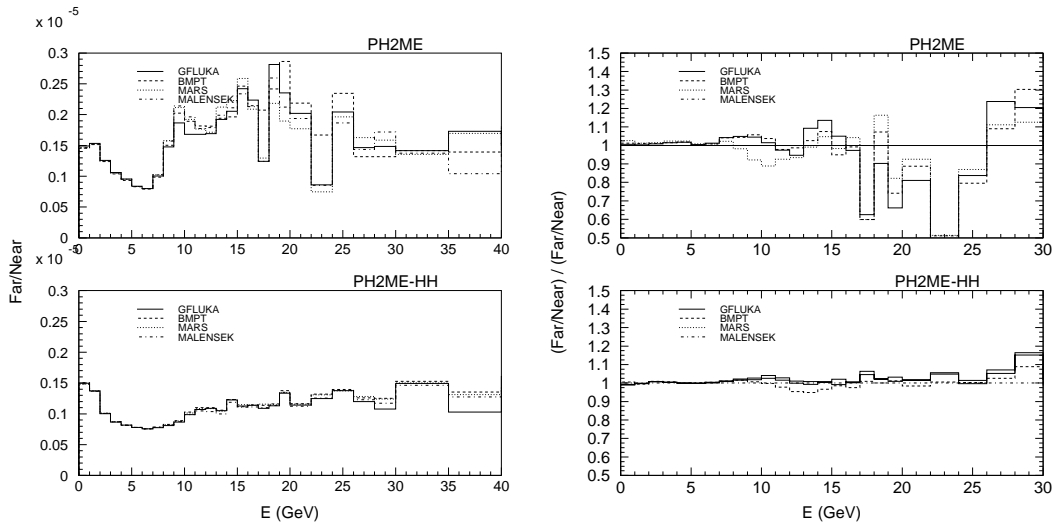


Figure 31: Left: The Far/Near ratio for the medium energy beam calculated using four models of hadron production on the NuMI target. Results for the hose-off (top) and hose-on (bottom) cases are shown. Right: Comparison of the Far/Near ratio for the various hadron production models relative to the Far/Near prediction from the GFLUKA model for the medium-energy beam. Results are shown for both the hose-off (top) and hose-on (bottom) cases.

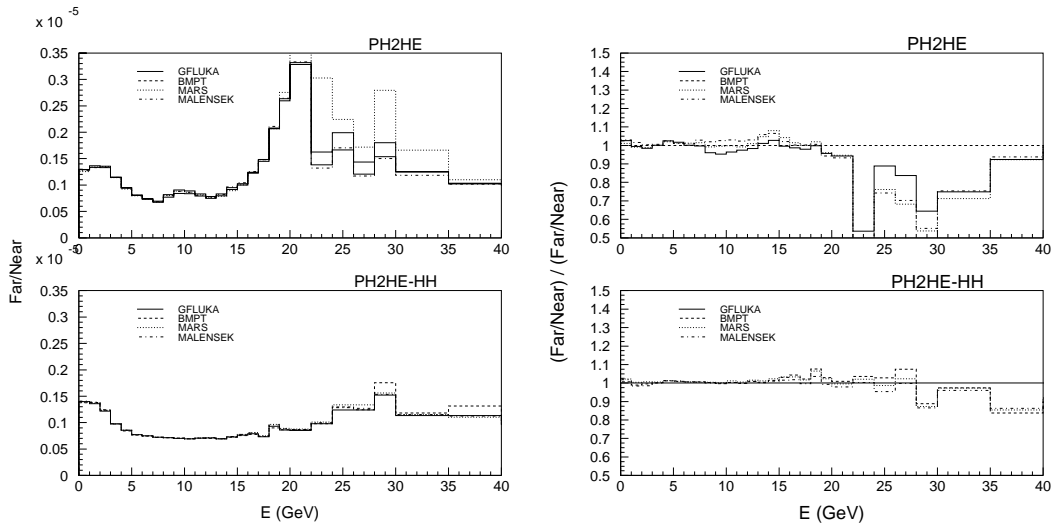


Figure 32: Right: The Far/Near ratio for the high energy beam calculated using four models of hadron production on the NuMI target. Results for the hose-off (top) and hose-on (bottom) cases are shown. Left: Comparison of the Far/Near ratio for the various hadron production models relative to the Far/Near prediction from the GFLUKA model for the high-energy beam. Results are shown for both the hose-off (top) and hose-on (bottom) cases.

$E$ (GeV)	Stat. Error (10 kt-yr)	F/N (%)		
		LE	LE-HH	LE/LE-HH
0 – 0.5	100%	6.0%	4.3%	1.4
0.5 – 1	25%	2.8%	1.8%	1.6
10 – 1.5	11%	1.2%	1.1%	1.1
1.5 – 2	8%	1.8%	1.8%	1.0
2 – 2.5	6%	1.1%	0.6%	1.8
2.5 – 3	5%	0.8%	0.2%	3.1
3 – 3.5	5%	0.2%	0.7%	0.3
3.5 – 4	5%	0.5%	0.9%	0.6
4 – 4.5	5%	0.9%	0.9%	1.1
4.5 – 5	7%	2.2%	1.4%	1.6
5 – 5.5	9%	4.7%	2.5%	1.9
5.5 – 6	10%	4.1%	3.7%	1.1
6 – 7	8%	4.2%	2.9%	1.5
7 – 8	8%	5.8%	2.4%	2.4
8 – 9	8%	5.7%	1.7%	3.3
9 – 10	9%	4.8%	2.3%	2.1
10 – 12	7%	8.3%	2.5%	3.3
12 – 14	7%	2.6%	1.1%	2.4
14 – 16	8%	8.3%	2.0%	4.1
16 – 18	8%	11%	1.3%	8.6
18 – 20	8%	12.5%	3.0%	4.1
20 – 25	6%	6.1%	1.1%	5.4
25 – 30	8%	32%	2.2%	15
30 – 40	8%	44%	13%	3.5

Table 5: Summary of the peak-to-peak spread in the prediction of the Far/Near ratio for the four models of hadron production considered as a function of energy for the low-energy beam. Results are shown for both the hose-off and hose-on cases.

$E$ (GeV)	Stat. Error (10 kt-yr)	Syst. Error		
		ME	ME-HH	ME/ME-HH
0 – 1	36%	1.5%	0.8%	1.8
1 – 2	11%	0.7%	0.3%	2.1
2 – 3	5%	0.8%	0.6%	1.4
3 – 4	3%	1.3%	0.4%	3.5
4 – 5	3%	1.5%	0.1%	17
5 – 6	3%	0.4%	0.2%	2.8
6 – 7	2%	0.7%	0.2%	3.4
7 – 8	2%	2.6%	0.7%	3.4
8 – 9	3%	3.6%	1.3%	2.8
9 – 10	4%	8.4%	1.4%	6.1
10 – 11	5%	9.8%	2.5%	4.0
11 – 12	6%	4.6%	2.8%	1.7
12 – 13	7%	3.4%	3.8%	0.9
13 – 14	7%	6.4%	3.9%	1.6
14 – 15	8%	6.7%	2.8%	2.4
15 – 16	8%	5.5%	2.1%	2.7
16 – 17	8%	4.0%	2.1%	1.9
17 – 18	3%	42%	3.3%	13
18 – 19	8%	13%	1.3%	9.9
19 – 20	10%	24%	1.9%	13
20 – 22	6%	11%	2.0%	5.3
22 – 24	8%	62%	2.8%	22
24 – 26	9%	14%	1.1%	13
26 – 28	11%	12%	3.6%	3.2
28 – 30	9%	14%	9.2%	1.5
30 – 35	8%	2.5%	2.2%	1.1
35 – 40	9%	29%	17%	1.7

Table 6: Summary of the peak-to-peak spread in the prediction of the Far/Near ratio for the four models of hadron production considered as a function of energy for the medium-energy beam. Results are shown for both the hose-off and hose-on cases.

$E$ (GeV)	Stat. Error (%) (10 kt-yr)	Syst. Error		
		HE	HE-HH	HE/HE-HH
0 – 1	45%	1.7%	1.1%	1.5
1 – 1	21%	1.6%	1.0%	1.6
2 – 3	12%	1.0%	1.2%	0.8
3 – 4	7%	0.4%	0.3%	1.2
4 – 5	5%	1.7%	0.9%	1.8
5 – 6	4%	1.0%	0.7%	1.4
6 – 7	3%	0.6%	0.4%	1.5
7 – 8	3%	1.8%	0.4%	4.6
8 – 9	2%	3.2%	0.2%	15
9 – 10	2%	4.0%	0.3%	13
10 – 11	2%	3.4%	0.7%	4.8
11 – 12	2%	2.6%	0.5%	5.2
12 – 13	2%	2.4%	0.8%	2.9
13 – 14	2%	2.9%	0.7%	4.3
14 – 15	2%	4.1%	1.2%	3.5
15 – 16	2%	2.7%	1.9%	1.4
16 – 17	2%	4.1%	2.3%	0.6
17 – 18	2%	1.7%	1.3%	1.3
18 – 19	3%	1.4%	4.2%	0.3
19 – 20	3%	3.6%	1.8%	2.0
20 – 22	3%	4.7%	1.7%	2.7
22 – 24	4%	64%	2.1%	31
24 – 26	6%	18%	3.9%	4.6
26 – 28	7%	24%	4.9%	4.9
28 – 30	7%	46%	10%	4.5
30 – 35	6%	24%	2.4%	10
35 – 40	7%	5.7%	13%	0.5

Table 7: Summary of the peak-to-peak spread in the prediction of the Far/Near ratio for the four models of hadron production considered as a function of energy for the high-energy beam. Results are shown for both the hose-off and hose-on cases.

## References

- [1] J. Hylen *et al.*, “Proposal to Include Hadronic Hose in the NuMI Beam Line”, NuMI-B-542, October 12, 1999.
- [2] J. Hylen *et al.*, “NuMI Hadronic Hose Technical Design Report”, NuMI-B-610, April 10, 1999.
- [3] The NuMI Technical Design Report, p. 2-28.
- [4] Atherton *et al.*, **CERN 80-07**, (1980).
- [5] Barton *et al.*, Phys. Rev. **27** (1983) 2580.
- [6] The SPY Collaboration, Eur. Phys. J. **C10** (1999) 605.
- [7] GEANT, CERN Program Library Long Writeup W5013 (1995).
- [8] A.J. Malensek, Fermilab-FN 341, (1981).
- [9] N.V. Mokhov and S.I. Striganov, “Model for Pion Production In Proton-Nucleus Interaction”, AIP Conf. Proc. **435** (1997) 543.
- [10] Alberto Marchionni, private communication, publication in process.